Validation and assessment of different RANS turbulence models for simulating turbulent flow through an orifice plate

Validation and assessment of different RANS turbulence models for simulating turbulent flow through an orifice plate

A P Jurga, M J Janocha*, G Yin, K E T Giljarhus and M C Ong

University of Stavanger, Stavanger 4036, Norway

* Contact author: marek.j.janocha@uis.no

Abstract. In the present study, numerical simulations using different Reynolds-Averaged Navier–Stokes (RANS) turbulence models are carried out to investigate the turbulent flow through the orifice plate at Reynolds number (Re) of 23000. The orifice thickness to pipe diameter ratio (t) and the orifice diameter to pipe diameter ratio (β) are fixed and equal to 0.1 and 0.5, respectively. The objective is to evaluate the behaviour of various RANS models with respect to the relevant flow parameters such as the pressure drop, velocity distributions and turbulence intensity profiles in the pipe by comparing the results with available published experimental data. The following turbulence models are studied: the $k-\varepsilon$, the $k-\varepsilon$ Low Re, the $k-\varepsilon$ RNG, the $k-\varepsilon$ Realizable, the $k-\omega$ SST, the γ – SST, the EARSM and the $k-\varepsilon$ Cubic models. It is found that based on the validation study of the flow through the orifice plate, the following models are in good agreement with experimental measurements: the $k-\omega$ SST, the γ – SST and the EARSM. They show a better performance than the $k-\varepsilon$ model family in predicting the flow features which are important for the orifice flowmeter design.

1. Introduction

Orifice plates next to venturi tubes and flow nozzles are among the most popular devices used for measurement and control of a fluid flow in a pipe. They are also frequently called differential pressure flowmeters as the principle of measurement is based on the differential pressure. In the orifice flowmeter, the differential pressure is created when the fluid flows through an artificial restriction (an orifice plate) placed in the cross section of the pipe, resulting in increased fluid velocity and, consequently, decreased pressure after passing the orifice plate. As per Section 4 of ISO 5167-2:2003 [2], the presence of the orifice plate causes a static pressure difference between the upstream (the high pressure) and the downstream (the low pressure) sides of the plate.

The pressure drop is measured at the wall pressure tappings, one on the upstream side and the other on the downstream side of the orifice plate located in a straight pipe [3]. Thus, the fluid flow in the pipe can be described using the Bernoulli's equation which allows calculating the flow rate through a pipe by using the measured differential pressure across the orifice. To get the actual velocity of the fluid, it is important to note that there are pressure losses due to frictional effects and due to the presence of the vena contracta area. To take into account both sources of pressure losses and calculate the real flow rate, the velocity behind the orifice is reduced by the discharge coefficient C_d (defined as the ratio between the actual and theoretical flowrate) which takes values smaller than 1 and is determined experimentally. The value of C_d depends on $\beta = d/D$ (where d is the orifice diameter and D is the pipe diameter) and the Reynolds number ($Re = UD/\nu$, where U is the flow velocity and ν is the kinematic viscosity of the

fluid) [1]. ISO 5167-2:2003 [2] refers to the standard orifice plate as shown in Figure 1, where it is stated that the diameter d shall, in all cases, be ≥ 12.5 mm and the diameter ratio $\beta = d/D$ shall always be ≥ 0.10 and ≤ 0.75 [2].

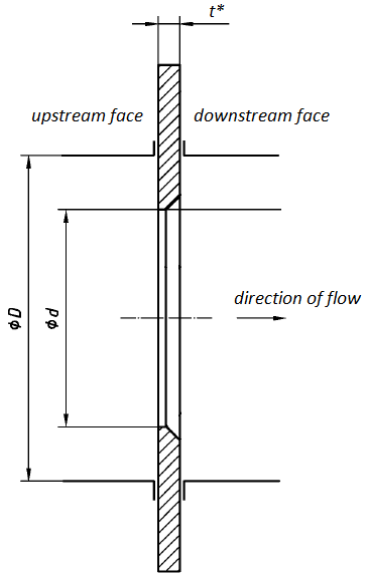

Figure 1. The cross-section of a standard orifice plate [2].

Although there are numerous investigators that have studied orifice flowmeters for different range of Reynolds numbers, the orifice thickness t^* and the orifice diameter to pipe diameter ratio β, for both laminar and turbulent flows, there are few numerical studies comparing the performance of different turbulence models for predicting the flow inside a pipe with an orifice flowmeter. This study is conducted to evaluate the performance of different RANS turbulence models by investigating flow characteristics through the orifice plate inserted in a straight pipe using series of Computational Fluid Dynamics (CFD) simulations. The simulations are carried out for the turbulent flow at Re = 23000 keeping the values of β and t ($t = t^*/D$) fixed.

2. Mathematical formulation and numerical method

2.1. Flow model

The present numerical models are solving three-dimensional steady Reynolds-averaged Navier-Stokes (RANS) equations of continuity and momentum as follows:

$$\frac{\partial u_i}{\partial x_i} = 0 \tag{1}$$

$$u_j \frac{\partial u_i}{\partial x_j} = -\frac{1}{\rho}\frac{\partial p}{\partial x_i} + \frac{\partial}{\partial x_j}\left[(v + v_T)\left(\frac{\partial u_i}{\partial x_j} + \frac{\partial u_j}{\partial x_i}\right)\right] \tag{2}$$

where i, j = 1, 2, 3 and x_i, x_j are coordinates of a Cartesian coordinate system, u_i is the time-averaged velocity components (u, v, w), p is the time-averaged pressure, ρ is the density of the fluid, v is the molecular viscosity and v_T is the turbulent eddy viscosity. Based on the Boussinesq assumption, the turbulent eddy viscosity describes the momentum transport caused by turbulent eddies as an analogy to the molecular viscosity. The Boussinesq assumption states that the Reynolds stress tensor ($\tau_{ij} = -\rho\overline{u_i u_j}$) is proportional to the trace-less mean strain rate tensor, as in Equation (3), where $\overline{u_i' u_j'}$ is

the time-average of the product of the fluctuating velocity components u_i' and u_j', k is the turbulence kinetic energy ($k = \overline{u_i' u_i'}/2$), δ_{ij} is the Kronecker delta.

$$\tau_{ij} = -\rho\overline{u_i' u_j'} = \rho v_T \left(\frac{\partial u_i}{\partial x_j} + \frac{\partial u_j}{\partial x_i}\right) - \frac{2}{3}\rho k \delta_{ij} \quad (3)$$

To compute the turbulent flows using the RANS equations, it is necessary to develop turbulence models that resolve the additional unknown Reynolds stresses. A common classification of RANS turbulence models is based on a number of additional transport equations that are solved simultaneously with Equations (1) and (2). Also, additional boundary conditions must be specified for the turbulence properties at the inlet and the outlet [1]. For example, for the $k-\varepsilon$ model, k and ε need to be specified in addition to the pressure and velocity boundary conditions. Since the appropriate values of these variables (k and ε) are not always known, a more useful option is to specify the turbulence intensity, I (ratio of the characteristic turbulent eddy velocity to the free-stream velocity) and the turbulent length scale, l (characteristic length scale of the energy contained in turbulent eddies) [1].

In the present study, the following turbulence models are employed and benchmarked: the linear models: the $k-\varepsilon$ [5], the $k-\varepsilon$ Low Re [7], the $k-\varepsilon$ RNG [8], the $k-\varepsilon$ Realizable [9], the $k-\omega$ SST [11], the γ – SST [18] models and the nonlinear explicit models: the EARSM [14] and the $k-\varepsilon$ Cubic [15] models, briefly described as below:

- The standard $k-\varepsilon$ model proposed by Launder and Spalding [5] solves two differential equations for two dependent variables: the turbulence kinetic energy, k [$\mathrm{m^2/s^2}$] and the rate of dissipation of the turbulence kinetic energy, ε [$\mathrm{m^2/s^3}$] [5]. The model gives reasonably accurate predictions at high Reynolds numbers in locations far from walls where the first cell lies in the log-law layer and the standard wall function is used. In the log-law layer, the relationship between the mean velocity and the distance from the wall is assumed as $u^+ = (1/\kappa)\ln(Ey^+)$, where u^+ is the mean wall-parallel velocity, $\kappa = 0.4$ is the von Karman's constant, $E = 9.8$ is the wall roughness parameter and y^+ is defined as $y^+ = (\Delta y u^*)/\nu$, where Δy is the distance from the wall to the cell center of the nearest computational cell and u^* is the friction velocity. When using the wall function, y^+ should be in the range of $30 < y^+ < 300$ to properly model the log-law layer [6].
- The $k-\varepsilon$ Low Re model is obtained by modifying the standard $k-\varepsilon$ turbulence model to take into account near-wall damping effects and the model replaces the dissipation rate with a modified dissipation rate introduced by Launder and Sharma [7]. For the wall-bounded flows, it is concluded that $k-\varepsilon$ Low Re model at low local Reynolds numbers in the near-wall region is more accurate than the standard $k-\varepsilon$ model. It requires near-wall treatment by introducing a wall function that allows the use of a more refined mesh near the wall to be able to capture flow characteristics within the viscous sublayer ($y^+ < 5$).
- The RNG model was developed using a mathematical technique called the renormalisation group (RNG) by Yakhot et al. [8] to renormalize the Navier-Stokes equations and systematically remove the smallest scales of the turbulence to a point where the remaining scales are resolvable with available computer capacities [8]. The model modifies the dissipation rate equation that accounts for the different scales of motions as opposed to the standard $k-\varepsilon$ model where the eddy viscosity is determined from a single turbulence length scale (only at the specified scale).
- The $k-\varepsilon$ Realizable model has been proposed by Shih et al. [9] and consists of a modified dissipation rate equation which is based on the transport equation of the mean-square vorticity fluctuation at high turbulent Reynolds numbers. Shih et al. [9] showed that the $k-\varepsilon$ Realizable model is a significant improvement over the standard $k-\varepsilon$.
- The $k-\omega$ SST model proposed by Menter [11] is a two-equation turbulence closure which combines the $k-\omega$ model in the near-wall regions and the $k-\varepsilon$ model in the fully turbulent region far from the walls so that the ε-equation is transformed into the ω-equation by

substituting $\varepsilon = k\omega$, where ω is the specific turbulence dissipation rate: $\omega = \varepsilon/k$ $[s^{-1}]$. The turbulent length scale here is defined as $l = \sqrt{k}/\omega$.

- The γ – SST model is a simplified Langtry-Menter 4-equation Transitional SST model [18]. The intermittency function (γ) and the momentum thickness Reynolds number (Re_θ) are coupled with the $k-\omega$ SST model [11]. The γ determines the percentage of time the flow is turbulent by acting on the turbulent kinetic energy transport equation in the SST model. The model is able to predict the laminar-turbulent transition process.
- The Explicit Algebraic Reynolds Stress Models (EARSM) model was developed by Hellsten [13] and Wallin et al. [14]. In contrary to the linear models using the Boussinesq assumption, the EARSM consists of the transport equations for the kinetic energy and an auxiliary quantity for the individual Reynolds stress anisotropies [14].
- The $k-\varepsilon$ Cubic model is a nonlinear two equation model introduced by Lien at el. [15] which allows the turbulence anisotropy to be predicted. However, the way in which the nonlinear model represents the interaction between the turbulence and the streamline curvature may not be adequate across the whole flow domain [15].

2.2. Numerical methods

In the present study, an open source finite volume method CFD code OpenFOAM v2012 is used to solve the governing equations of the fluid flow. A steady state solver simpleFoam which employs the Semi-Implicit Method for Pressure Linked Equations (SIMPLE) is used for the pressure-velocity coupling solution. Second order discretization schemes are used for the convective and diffusive terms.

3. Computational sep

3.1. Computational domain

The computational domain topology for the straight pipe simulations is shown in Figure 2. The pipe diameter is set as D = 1m. The distance between the pipe inlet and outlet for the straight pipe is set to L = 50D (Figure 2). The computational domain topology for the straight pipe with the orifice plate is shown in Figure 3. The pipe diameter is set as D = 1m. The distance between the pipe inlet and the front face of the orifice plate is set to Lu = 5D and the distance between the pipe outlet and the back face of the orifice plate is set to Ld = 10D (Figure 3). The cross sections 1 and 2 are the two locations marked in Figure 3, where the centerline pressure values are measured to obtain the discharge coefficients and their distances to the front and back face of the orifice plate are the same as in Nitter et al. [16]. The orifice thickness is set to t^* = 0.1m and the orifice to pipe diameter ratio is set to β = 0.5.

The inlet boundary condition for the straight pipe simulations is a uniform flow with (u, v, w) = (1 m/s, 0, 0). The value of k is calculated as $k = 1.5(uI)^2$ where I is the turbulence intensity estimated as $I = 0.16(Re)^{-1/8}$. The inlet values of ε, ω and γ are calculated according to the recommended expressions given in the corresponding reference papers in Section 2.1. The pressure is set as a zero normal gradient at the inlet. At the outlet, the three velocity components as well as the variables: k, ε, ω, γ (depending on the model used) are set as the zero normal gradient and the reference pressure is set as zero. The simulated turbulent velocity profile at the outlet of the straight pipe is then used as the inlet boundary condition for the pipe with the orifice plate simulations as shown in Figure 4, which is the same approach as the one used by Nitter et al. [16]. The same fully developed inlet velocity profiles are used for the mesh convergence and validation studies. The inlet values of k, ε, ω or γ for the orifice pipe simulations are also imposed by using the fully developed outlet profiles from the precursor simulations of the corresponding straight pipe cases. The pressure is set as the zero normal gradient at the inlet of the pipe with the orifice plate. At the outlet of the pipe with the orifice plate, the boundary conditions are set to be the same as for the outlet of the straight pipe. On the surface of the pipe wall and the orifice plate, a no-slip boundary condition is prescribed with (u, v, w) = (0, 0, 0).

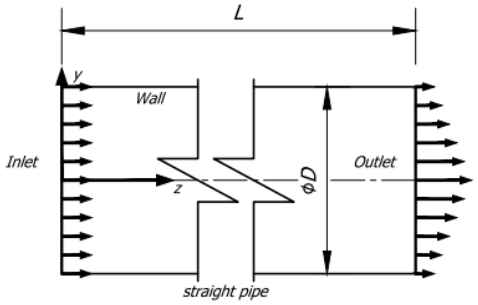

Figure 2. The computational domain for the straight pipe simulations [16].

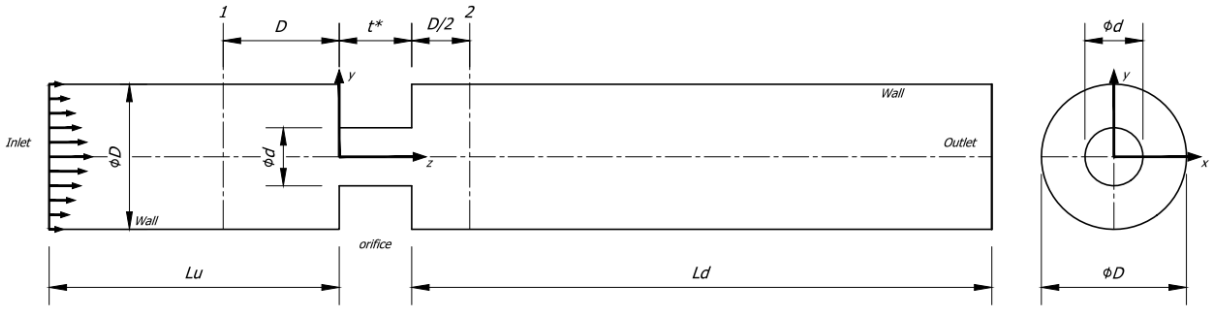

Figure 3. The computational domain for the straight pipe with the orifice plate simulations.

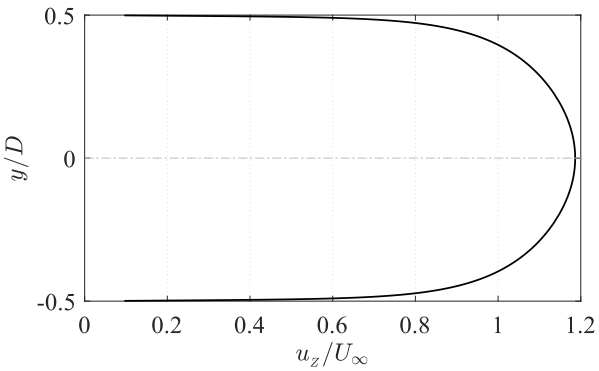

Figure 4. An example of the radial profile of the normalised axial velocity upstream of the orifice plate at the inlet (outlet of the straight pipe precursor simulation) applied in the mesh convergence study at Re = 40000 using k − ω model.

3.2. Convergence study

The convergence studies are carried out to determine the required spatial resolution of the computational mesh for the orifice case with $t = 0.25$ ($t = t^*/D$) and $\beta = 0.5$ at $Re = 40000$. A set of three geometrically similar meshes is generated using a constant refinement factor r = 1.25 and presented in Table 1. An example of the mesh distribution is shown in Figure 5. The mesh is refined close to the walls of the domain to ensure that the $y^+ < 1$. The distributions of the normalized velocity along the centerline in Figure 6 and the pressure along the centerline in Figure 7 is used to assess the mesh convergence. A good agreement is found between the results obtained on the dense: M2 and very dense: M3 mesh variants, indicating that the M3 can be considered to provide the mesh independent solution of the turbulent flow in the present study.

Table 1 Mesh resolutions for convergence study

Mesh	Number of cells
M1	2703032
M2	5313792
M3	8997648

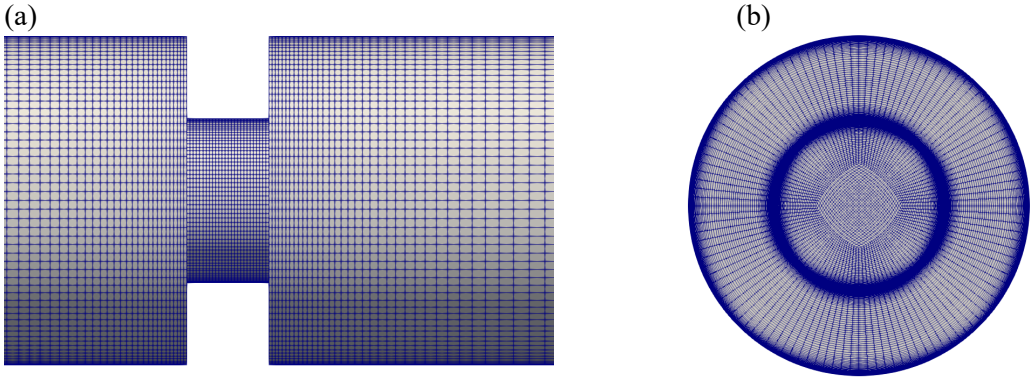

Figure 5. An example of the mesh M1 for t = 0.25 and β = 0.5 in (a) the YZ plane and (b) the XY plane.

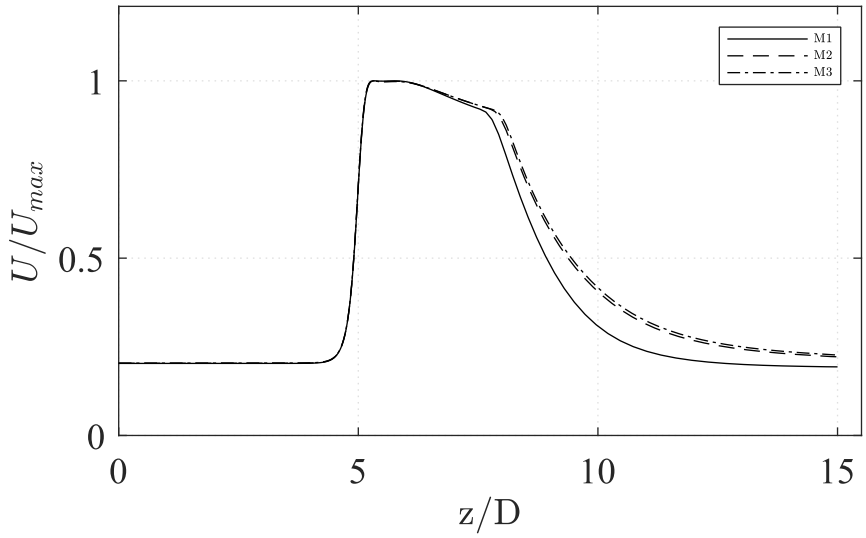

Figure 6. The normalised streamwise velocity along the centerline at Re = 40000 with t = 0.25 and β = 0.5 for the investigated mesh density variants: solid: M1, dashed: M2 and dash-dotted: M3.

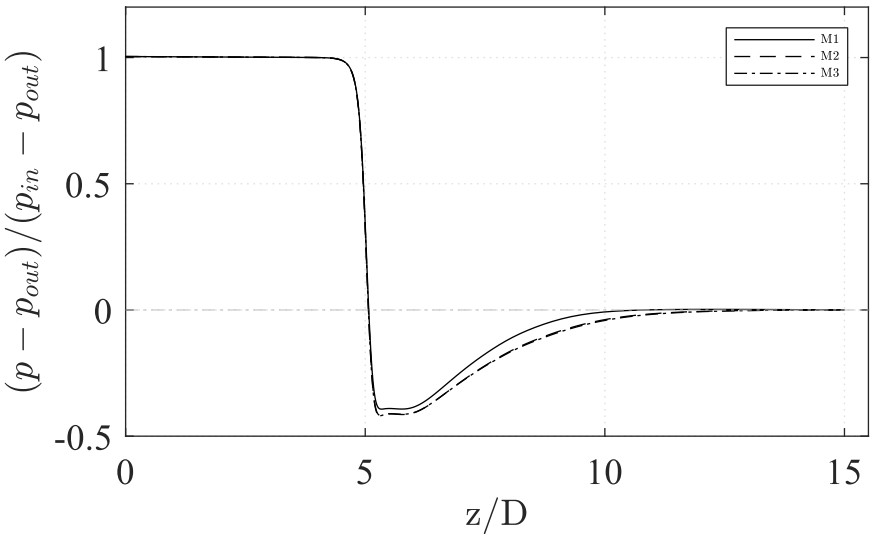

Figure 7. The normalised pressure profiles along the centerline at Re = 40000 with t = 0.25 and β = 0.5 for the investigated mesh density variants: solid: M1, dashed: M2 and dash-dotted: M3.

4. Results and discussion

A series of numerical simulations using the same grid resolution of the very dense mesh described in Section 3.2, is performed using different RANS models briefly described in Section 2. In this study, the numerical simulations are carried out at Re = 23000 keeping the value of β and t fixed as follows: β = 0.5 and t = 0.1. The results from the numerical simulations are compared with the experimental data reported by Fiorini [17] and Utanohara et al. [10] for the case of the straight pipe without and with the orifice, respectively. Fiorini [17] conducted the experimental investigation of the turbulent pipe flow at high Reynolds numbers ranging 6500 < Re < 38000. The pressure profiles in Figure 8 and the normalized mean velocity profiles in Figure 9 for the straight pipe show that the following models: the $k-\omega$ SST, the γ – SST, the EARSM, the $k-\varepsilon$ Cubic and the $k-\varepsilon$ Low Re achieve good agreement with the Fiorini's measurements. However, the $k-\varepsilon$ Cubic and the $k-\varepsilon$ Low Re models do not show good performance when compared to the experimental LDV (Laser Doppler Velocimetry) data published by Utanohara et al. [10] as shown in Figure 10 - Figure 15. The axial velocity profiles downstream the orifice predicted by the $k-\omega$ SST, the γ – SST and the EARSM models are in good agreement with the experimental results as presented in Figure 10, Figure 12 and Figure 14. Also the shapes of the turbulence intensity profiles predicted by the $k-\omega$ SST, the γ – SST and the EARSM models are qualitatively similar to the shapes of the experimental profiles in Figure 11, Figure 13 and Figure 15. Figure 16 shows streamlines plotted on the y-z plane located in the longitudinal axis of symmetry of the pipe with the orifice based on the flow fields predicted by all the investigated turbulence models. The $k-\omega$ SST, the γ – SST, the EARSM, the k-ε RNG, and the k-ε Realizable show similar size of the recirculation bubble. The recirculation bubble predicted by the $k-\varepsilon$ Low Re, the standard $k-\varepsilon$ and the Cubic $k-\varepsilon$ is significantly smaller than aforementioned models. Thus, it is concluded that there are three models: the $k-\varepsilon$ SST, the γ – SST and the EARSM showing superior performance with respect to simulating the turbulent flow through the straight pipe and through the orifice flowmeter.

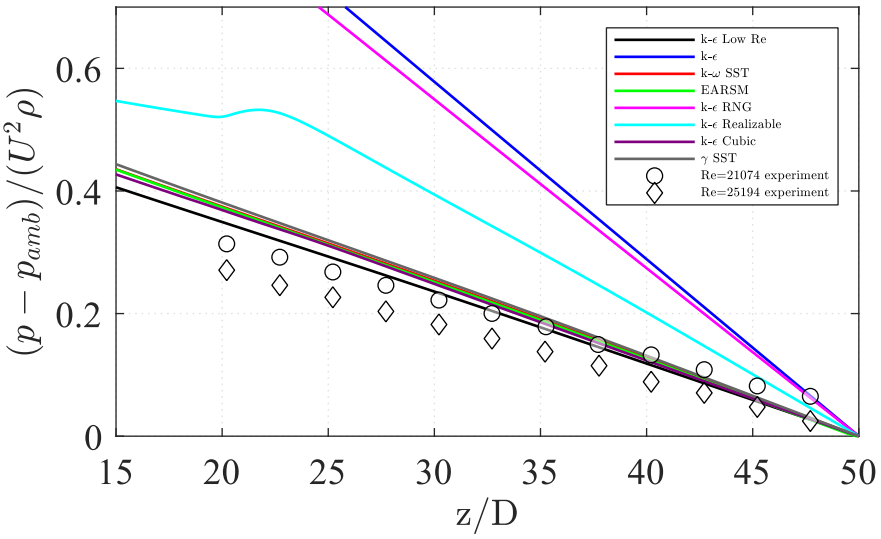

Figure 8. The pressure profiles along the centerline at Re = 23000 compared with the experimental data reported by Fiorini [17] between Re = 21074 and Re = 25194 for different turbulence models in the straight pipe.

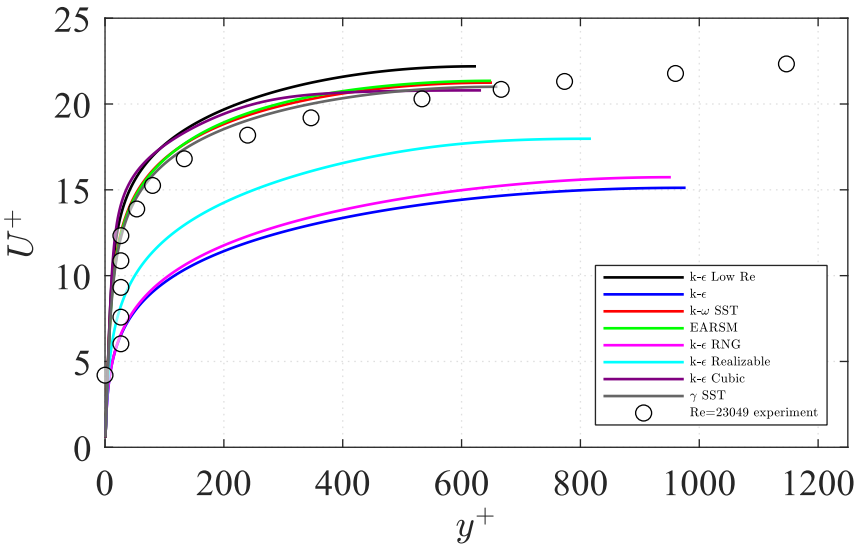

Figure 9. The normalized mean velocity profiles at Re = 23000 compared with the experimental data reported by Fiorini [17] for Re = 23049 for different turbulence models in the straight pipe.

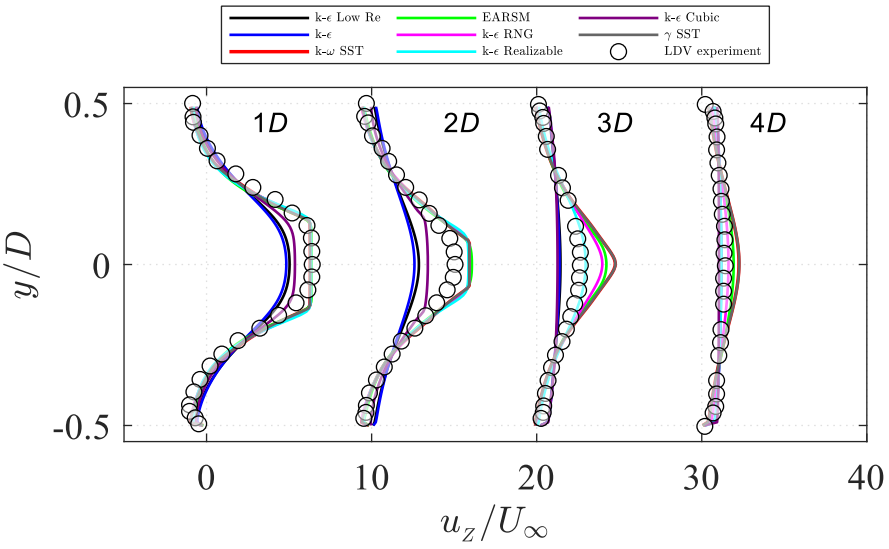

Figure 10. The axial velocity profiles at the distance z = 1D, 2D, 3D and 4D downstream from the orifice at Re = 23000 at scale 0 - 10 for each z/D (only the first set of lines conforms to the scale and subsequent sets are offset by u_z/U_∞ = 10 from each other).

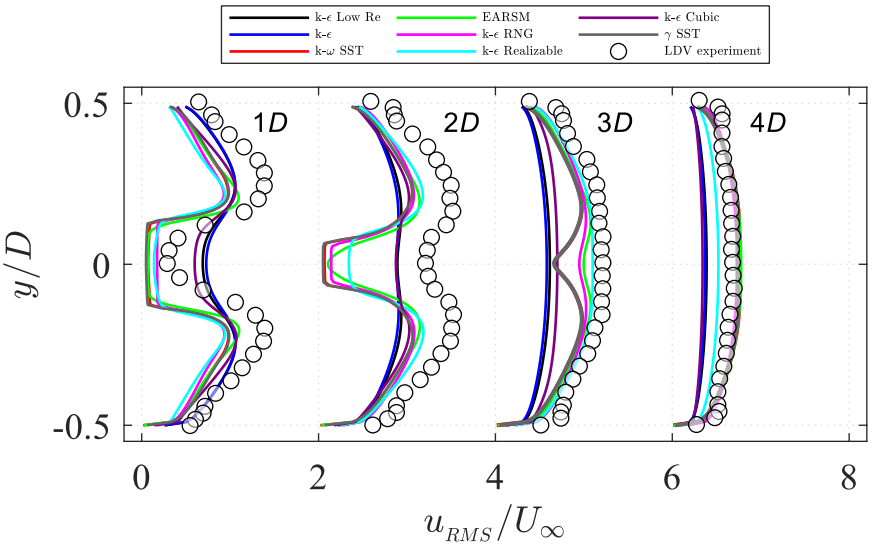

Figure 11. The turbulence intensity profiles at the distance z = 1D, 2D, 3D and 4D downstream from the orifice at Re = 23000 at scale 0 - 2 for each z/D (only the first set of lines conforms to the scale and subsequent sets are offset by u_{RMS}/U_∞ = 2 from each other).

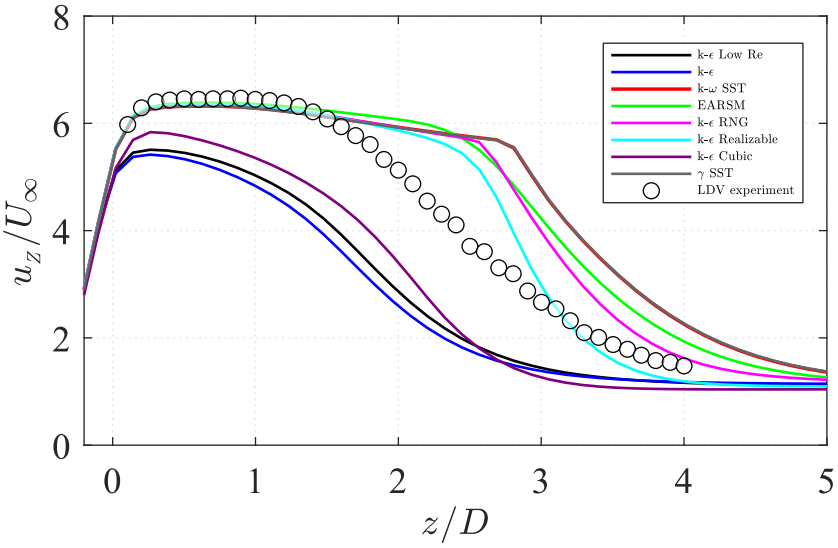

Figure 12. The axial velocity profiles along the centerline downstream from the orifice at Re = 23000.

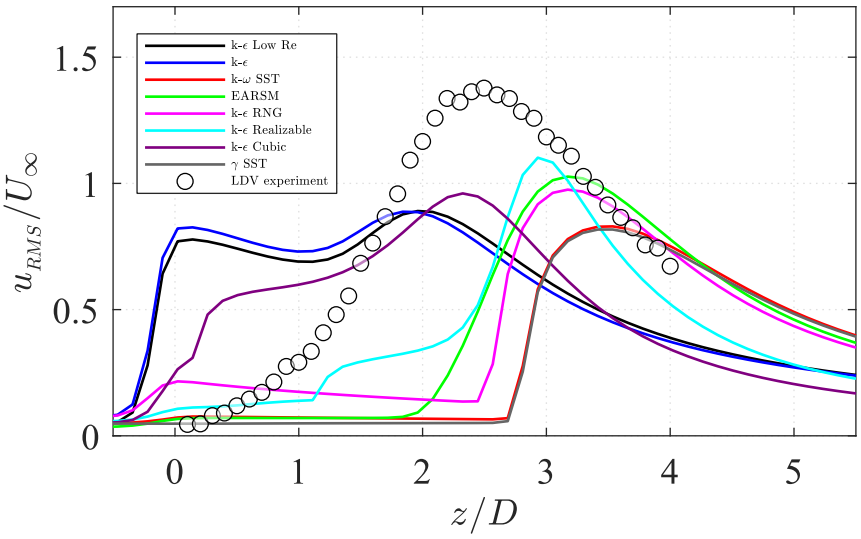

Figure 13. The turbulence intensity profiles along the centerline downstream from the orifice at Re = 23000.

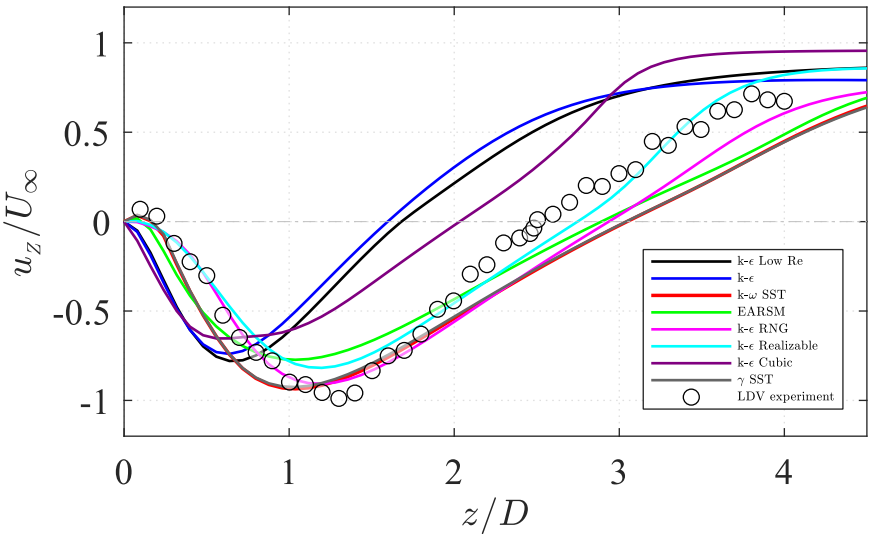

Figure 14. The axial velocity profiles near the wall (y = 1 mm from the wall) downstream from the orifice at Re = 23000.

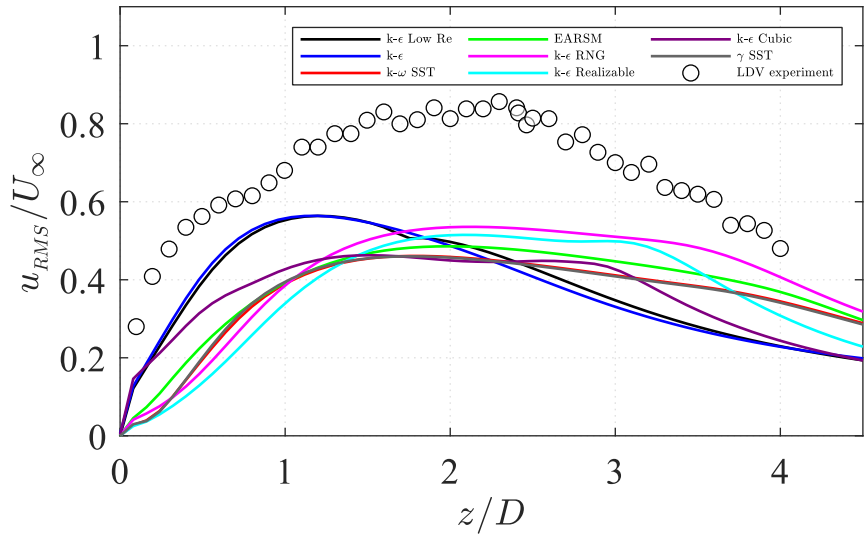

Figure 15. The turbulence intensity profiles near the wall (y = 1 mm from the wall) downstream from the orifice at Re = 23000.

(a)

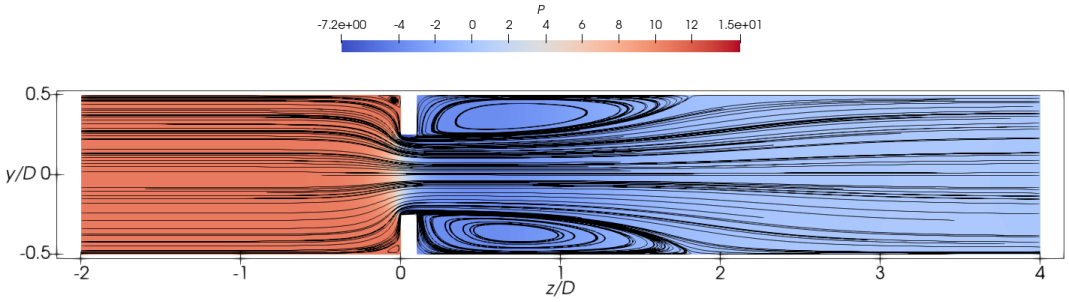
P
-7.2e+00 -4 -2 0 2 4 6 8 10 12 1.5e+01
0.5
y/D 0
-0.5
-2 -1 0 1 2 3 4
z/D

(b)

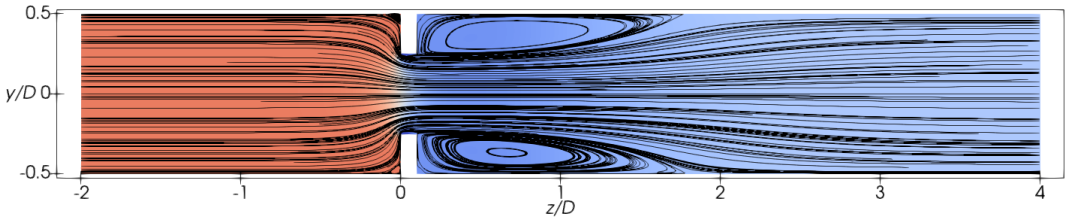
0.5
y/D 0
-0.5
-2 -1 0 1 2 3 4
z/D

(c)

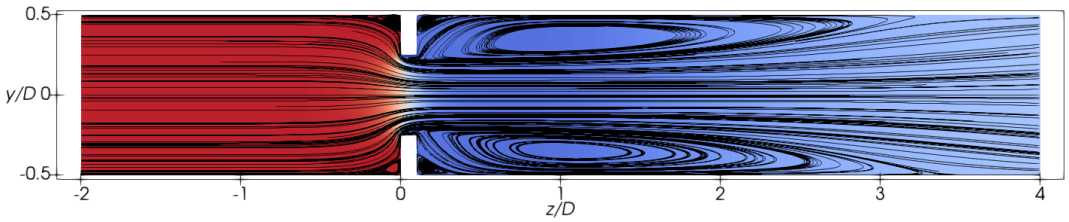
0.5
y/D 0
-0.5
-2 -1 0 1 2 3 4
z/D

(d)

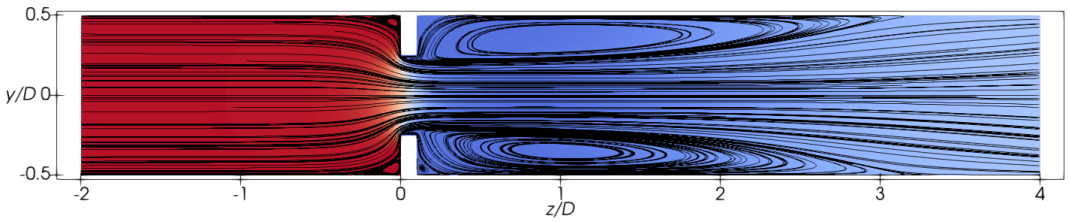
0.5
y/D 0
-0.5
-2 -1 0 1 2 3 4
z/D

(e)

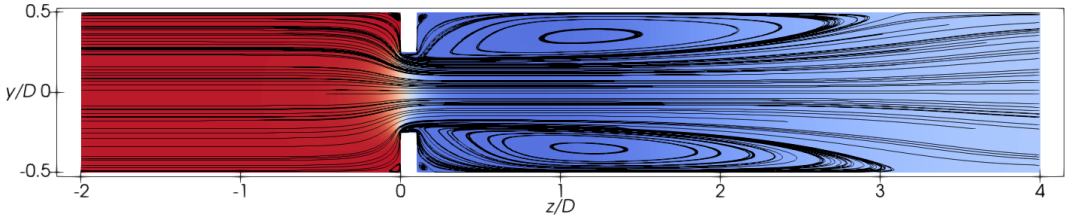
0.5
y/D 0
-0.5
-2 -1 0 1 2 3 4
z/D

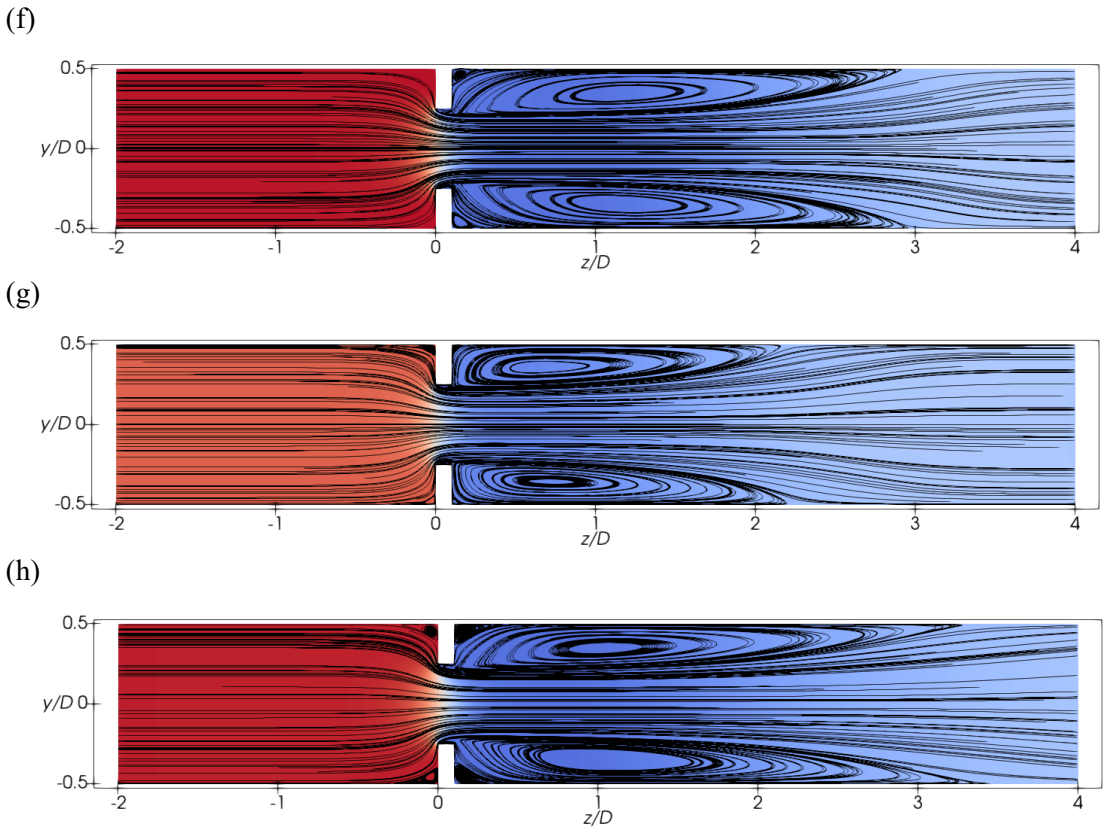

Figure 16. The separation flow regions predicted by (a) the $k-\varepsilon$ Low Re, (b) the $k-\varepsilon$, (c) the $k-\omega$ SST, (d) the EARSM, (e) the $k-\varepsilon$ RNG, (f) the $k-\varepsilon$ Realizable, (g) the $k-\varepsilon$ Cubic and (h) the γ – SST.

The value of the discharge coefficient (C_d) given by Equation (4) is calculated in the same way as given by Nitter et al. [16], where $\Delta P^* = \Delta P/\rho U^2$ is the non-dimensional pressure drop, ΔP is the difference of the pressure value between the cross sections 1 and 2 as shown in Figure 3, U is the inlet mean velocity (1m/s) and ρ is the density of the fluid (for the incompressible flow: ρ = 1kg/m^3). The highest predicted value of the discharge coefficient, as shown in Table 2, is given by the $k-\varepsilon$, the $k-\varepsilon$ LS and the $k-\varepsilon$ Cubic models, which is related to the lower predicted pressure differences compared to those predicted by the $k-\omega$ SST, the EARSM, the $k-\varepsilon$ RNG, the $k-\varepsilon$ Realizable and the γ – SST models, where there is no significant variation between the predicted discharge coefficients. According to Table A.2 of Annex A from ISO 5167-2:2003 [2] the discharge coefficient for the orifice with *D* and *D/2* tappings as a function of β, Re and $D \geq 71.12$ mm is given as approximately 0.61 which is very close to the one obtained using the EARSM turbulence model. The percentage error between the C_d = 0.6164 from the numerical simulation with the EARSM model and the one given by ISO is approximately 1 %.

$$C_d = \frac{1}{\sqrt{2}}\left(\frac{1}{\beta}\right)^2 \sqrt{1-\beta^4}\,\frac{1}{\sqrt{\Delta P^*}} \tag{4}$$

Table 2 Discharge coefficient C_d for Re = 23000 (t = 0.1, β = 0.5).

Turbulence model	C_d [-]
$k-\varepsilon$ LS	0.7260
$k-\varepsilon$	0.7382
$k-\omega$ SST	0.6244
EARSM	0.6164
$k-\varepsilon$ RNG	0.6242
$k-\varepsilon$ Realisable	0.6230
$k-\varepsilon$ Cubic	0.6886
γ – SST	0.6243

5. Conclusion

In the present study, the CFD simulations are performed to investigate the flow behavior through the orifice plate using different turbulence models. The numerical study is based on RANS equations for the turbulent flow at Reynolds number of 23000. Eight different RANS turbulence models are used to resolve the turbulent stress and their performances are evaluated.

The turbulent flow profiles through the straight pipe are used as the inlet profiles for the orifice in the pipe flow simulations. The simulation set up is based on the experiments on the orifice flow reported by Utanohara et al. [10]. The predicted results show better agreement with the experimental data of the velocity distribution than with the turbulence intensity profiles. The main conclusion based on the present work is that the turbulence models: the $k-\omega$ SST, the γ – SST and the EARSM models produce similar results that are in a fair agreement with the experimental data. Although the turbulence models based on the Boussinesq eddy viscosity assumption are typically used in the flows through pipes, the EARSM model shows the best performance for simulating the fully developed turbulent flow through the orifice plate as supported by the presented comparisons with the experimental data. The EARSM's assumption of anisotropic Reynolds stress tensor gives superior results in capturing both separation regions of the flow behind the orifice plate as well as predicting the effect of the curvature of the mean flow.

References

[1] Cengel Y A and Cimbala J M 2014 *Fluid Mechanics Fundamentals and Applications, 3rd Ed.* (New York: McGraw-Hill) p 1031.
[2] ISO 5167-2:2003 Measurement of fluid flow by means of pressure differential devices inserted in circular cross-section conduits running full — Part 2: Orifice plates.
[3] ISO 5167-1:2003 Measurement of fluid flow by means of pressure differential devices inserted in circular cross-section conduits running full — Part 1: General principle and requirements.
[4] Reader-Harris M 2015 *Orifice Plates and Venturi Tubes.* (London: Springer).
[5] Launder B E and Spalding D B 1974 The numerical computation of turbulent flows, *Comput. Methods Appl. Mech. Eng.* **3**(2), 269-289.
[6] Versteeg H K and Malalasekera W 2007 *An introduction to computational fluid dynamics: The finite volume method 2nd Ed.* (Harlow: Pearson Education).
[7] Launder B E and Sharma B I 1974 Application of the energy-dissipation model of turbulence to the calculation of flow near a spinning disc, *Lett. Heat Mass Transfer*, **1**, 131-38.
[8] Yakhot V, Orszag S A, Thangam S and Speziale C G 1992 Development of Turbulence Models for Shear Flows by a Double Expansion technique, *Phys. Fluids A Fluid Dyn*. **4**(7).
[9] Shih T H, Liou W W, Shabbir A, Yang Z and Zhu J 1995 A New k- ε Eddy Viscosity Model For High Reynolds Number Turbulent Flows, *Comput. Fluids*, **24**(3), 227-38.
[10] Utanohara Y, Nagaya Y and Nakamura A 2012 Influence of Local Field on Flow Accelerated Corrosion Downstream from an Orifice, *J. Power Energy Syst.* **6**(1), 18-33.
[11] Menter F R 1994 Two-Equation Eddy-Viscosity Turbulence Models for Engineering

Applications, *AIAA J*. **32**(8), 1598-605.
[12] Langtry R B 2006 *A Correlation-Based Transition Model using Local Variables for Unstructured Parallelized CFD codes.* University of Stuttgart, PhD Thesis.
[13] Hellsten A 2005 New Advanced k-omega Turbulence Model for High-Lift Aerodynamics, *AIAA J*. **43**(9), 1857-1869.
[14] Wallin S and Johansson A V 2000 An Explicit Algebraic Reynolds Stress Model for Incompressible and Compressible Turbulent Flows, *J. Fluid Mech.* **403**, 89-132.
[15] Lien F S, Chen W L and Leschziner M A 1996 Low-Reynolds-Number Eddy-Viscosity Modelling Based on Non-Linear Stress-Strain/Vorticity Relations *Proc. 3rd Symp. On Engineering Turbulence Modelling and Measurements*, (Crete, Greece: May 27 – 29, 1996) Eds Rodi W and Bergeles G (Elsevier Series in Thermal and Fluid Sciences) vol 3.
[16] Yin G, Nitter B and Ong M C 2021 Numerical Simulations of Turbulent Flow Through an Orifice Plate in a Pipe, *J. Offshore Mech. Arct. Eng.* **143**(4), 041903-041914.
[17] Fiorini T 2017 *Turbulent Pipe Flow - High Resolution Measurements in CICLoPE*. University of Bologna, PhD Thesis.
[18] Langtry R B and Menter F R 2009 Correlation-Based Transition Modeling for Unstructured Parallelized Computational Fluid Dynamics Codes, *AIAA J*. (**47**)12, 2894-906.